Combination of Sentinel-2 and MODIS for Enhanced Thermal Data Resolution. Case study in Bragança, Portugal (2018–2023)

Cátia Rodrigues de Almeida[1,2,3]; João Alírio[1,2]; Artur Gonçalves[3]; Ana Cláudia Teodoro[1,2]

[1]Department of Geosciences, Environment and Land Planning, Faculty of Sciences, University of Porto, Rua Campo Alegre, 687, 4169-007 Porto, Portugal; up201600831@fc.up.pt; joao.m.alirio@gmail.com; amteodor@fc.up.pt
[2]Earth Sciences Institute (ICT), Pole of the FCUP, University of Porto, 4169-007 Porto, Portugal;
[3]CIMO, LA SusTEC, Instituto Politécnico de Bragança, Campus de Santa Apolónia, 5300 253 Bragança, Portugal, ajg@ipb.pt

Keywords: Remote Sensing (RS), Land Surface Temperature (LST), Thermal data, Data resampling, Google Earth Engine (GEE), Urban Heat Island (UHI)

Abstract

Remote Sensing data are used across various fields, and their selection must consider the study's objectives, sensor capabilities, and different resolutions. In urban climate investigations, such as the Urban Heat Island (UHI), thermal sensors estimate Land Surface Temperature (LST), but freely available products have low spatial resolution. This study proposes a methodology to resample MODIS LST from 1 km to 10 m (MODIS_LST_1km and MODIS_LST_10m, respectively), between 2018 and 2023, in different seasons, along the border between Portugal and Spain. We used Google Earth Engine to calculate MODIS_LST_1km and the Normalized Difference Vegetation Index (NDVI) from Sentinel-2. We resampled the NDVI to 1 km and calculated a regression equation for each data when images from both products were available. We applied the resulting equation using NDVI with a 10 m (original resolution) to obtain MODIS_LST_10m. We validated the results with Landsat-8 LST (Landsat_LST) data through Spearman correlation in R software. Additionally, we analyzed the correlation between NDVI and the Enhanced Vegetation Index (EVI) from Landsat-8 with MODIS_LST_10m to assess whether higher temperatures corresponded to areas with low vegetation. The model showed good explainability, especially in summer, and validation with Landsat-8 was also more significant in summer (ρ between 0.736 and 0.895). The correlations between MODIS_LST_10m with EVI and NDVI were negative on most dates, indicating higher temperatures in less vegetated areas. For future studies, we plan to test other sensors/satellites, such as Sentinel-3, to reinforce the robustness of this methodology.

1. Introduction

The application of Remote Sensing (RS) data in scientific analyses is extensive, encompassing areas such as environmental monitoring, Land Use and Land Cover (LULC) analysis, climate studies (Dousset and Gourmelon, 2003; Luvall *et al.*, 2015). The Urban Heat Island (UHI) effect is one of the topics in which RS has been widely employed (Almeida *et al.*, 2022, 2021). It is characterized by higher temperatures in urbanized areas when compared with the surrounding vegetated regions (Imhoff *et al.*, 2010; Oke, 1982), and it can affect the local microclimate and biome, the population's well-being, contribute to the dispersion of atmospheric pollutants, enhance biological risks, among other effects (Agam *et al.*, 2008; Dousset and Gourmelon, 2003; EPA - United States Environmental Protection Agency, n.d.; Hall *et al.*, 2012; Mirzaei *et al.*, 2020; Oke, 1982; Weng *et al.*, 2004). This effect can also be approached from the Surface Urban Heat Island (SUHI) perspective, evaluating the temporal variability of differences in Land Surface Temperature (LST) between rural and urban contexts (Voogt and Oke, 2003; Weng and Fu, 2014).

One of the methodologies for analyzing the SUHI encompasses using RS data. This approach uses the average radiometric temperature of surface components within the field of view of thermal sensors (Guillevic *et al.*, 2018; Hulley *et al.*, 2019). These sensors record information in the spectral range of the atmospheric window (between 8 and 14 μm) and, to perform the measurement, are cooled to temperatures close to 0º K (so that their internal temperature does not interfere with the recording). They then average the temperatures of objects within their field of view, compare them with internal reference temperatures (representing absolute radiation), and provide the data that will later be used by researchers (Imhoff *et al.*, 2010).

The most commonly used LST products come from the Landsat satellites (since Landsat 4), Terra, Aqua, Meteosat Second Generation (MGS), and the Geostationary Operational Environmental System (GOES) *(Almeida et al., 2021; Zhou et al.*, 2019). The selection depends on the study's objective. There are two fundamental scales for studies using LST: i) the spatial scale, which defines the smallest size of objects that the sensor can distinguish (e.g., 10m, 30m, 1 km); and ii) the temporal scale, which indicates the frequency with which the sensor acquires images of the same area (e.g., daily, weekly) (Lillesand *et al.*, 2015). These scales present significant challenges for study areas not covered by geostationary satellites, which continuously acquire data from an exact location.

In the literature, various methodologies have been proposed to improve the spatial resolution of LST from different satellites using different resampling techniques (Bisquert *et al.*, 2016; Sánchez *et al.*, 2020). Among the proposed models, linear regressions between LST and Visible and Near-Infrared (VNIR) bands, Neural Networks (NN), and Data Mining (DM) algorithms stand out. However, the results obtained with linear regression have proven more robust (Sánchez *et al.*, 2020). The use of Vegetation Indices (VI), such as the Normalized Difference Vegetation Index (NDVI) and Enhanced Vegetation Index (EVI), derived from sensors with higher spatial resolution, combined with LST data from sensors with higher temporal resolution, like Moderate Resolution Imaging Spectroradiometer (MODIS), offers an opportunity to enhance the spatial resolution, making them more suitable for detailed analyses, especially in areas with LULC transitions over short distances (Tomlinson *et al.*, 2011).

This contribution has been peer-reviewed. The double-blind peer-review was conducted on the basis of the full paper.
https://doi.org/10.5194/isprs-annals-X-G-2025-729-2025

VIs can also be used to identify the density and health of vegetation in a given location, providing the ability to understand LULC composition. Studies show that there is an inverse correlation between VIs and LST, indicating that areas with more vegetation tend to have lower LST, while areas with less vegetation tend to have higher LST (Bokaie *et al.*, 2019; Grover and Singh, 2016; Miura *et al.*, 2001). NDVI and EVI are VIs used in studies to understand the local microclimate, such as UHI. Both indices range from -1 to +1, where values below zero represent clouds or water bodies, and values near +1 represent fully vegetated. EVI is an enhanced version of NDVI as it corrects for atmospheric and soil interferences, making it recommended for areas with high biomass (Gaitán *et al*., 2013; Rouse *et al.*, 1973).

It is worth noting that seasonality is a factor that influences the behaviour and metabolism of vegetation, the colour of its leaves, and consequently its reflectance, and it should be considered during data processing to achieve a more detailed analysis (Mariën *et al.*, 2019). In seasons with higher solar radiation availability and elevated temperatures (such as spring and summer), vegetation tends to be more active, and consequently, vegetation indices (VIs) show higher values. The contrast between LST values and surfaces with anthropogenic materials and low albedo is also higher. In autumn and winter, VIs scores tend to decrease gradually due to reduced photosynthetic activity, which leads to the senescence period in some species, such as deciduous trees. During this time, the average daily temperature is also lower, minimizing the contrasts in LST and VI values (Johnson *et al.*, 2018; Mariën *et al.*, 2019; Pettorelli *et al.*, 2005).

Considering this context, our objective is to propose a methodology that utilizes data from the MODIS sensor aboard the Terra satellite, which has a spatial resolution of 1 km and resampled it to 10 m (MODIS_LST_1km and MODIS_LST_10m, respectively). We chose this sensor for its high temporal resolution, acquiring data once every day or two days (NASA, n.d.). In addition to MODIS data, we also used Sentinel-2 data to build the model proposed in this methodology and the LST from Landsat-8 (Landsat_LST) for validation. The proposed method focused on images collected in the border region between Portugal and Spain from 2018 to 2023.

Additionally, we performed correlations between the NDVI and EVI from Landsat-8 to assess whether the higher temperatures from MODIS_LST_10m were associated with LULC types with lower vegetation indices or anthropogenic characteristics. Our hypotheses are that: (a) by improving the spatial resolution of MODIS data, we will be able to produce more detailed results for analyzing surface thermal behaviour in the study area concerning its land use and land cover (LULC) composition; and (b) we will be able to assess thermal behaviour using vegetation indices (VIs), which will likely show a negative correlation, as locations with a more extensive vegetation cover tend to have more regulated land surface temperatures (LST).

2. Methodology

2.1 Study Area

We delimited the study area near the border limits between Portugal and Spain, covering the municipalities of Bragança, Mirandela, Macedo de Cavaleiros, Chaves, and Verín (Figure 1). We have already analyzed the UHI effect in Bragança using thermal data from different sensors, including MODIS, whose results were limited due to its spatial resolution (1 km) (Almeida *et al.*, 2023a, 2023b, 2022). To apply the proposed methodology in this research, we expanded the study area to include neighbour municipalities to gather more data, improve the model's level of detail, and incorporate different LULC types, such as forest areas, agricultural lands, rural and urban zones, etc. We focused on describing the most relevant areas within this extension, as the primary objective was to identify the method instead of performing a detailed classification of the evaluated areas.

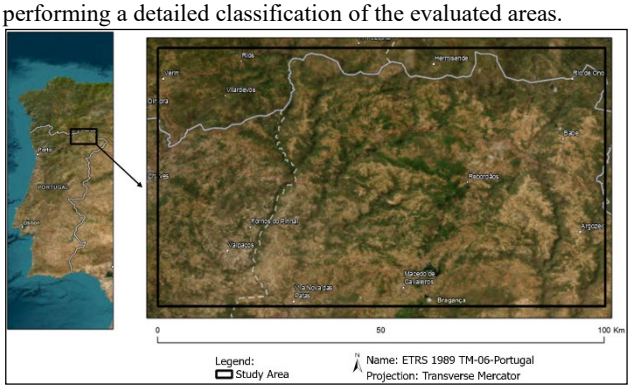

Figure 1. Delimitation of the study area along the border between Portugal and Spain (black rectangle)

The municipality of Bragança is located in the extreme northeast of Portugal's mainland (41º48'20" N, 6º45'42" W). It has 35,341 inhabitants (in 2021) and an area of approximately 1,174 km² (Bragança, n.d.; INE, n.d.). It is located in a mountainous region with complex terrain due to elevation variation (Gonçalves *et al.*, 2018). The LULC is heterogeneous, with urban fabric, agriculture, forest, shrublands, natural, and bare land. According to the Köppen-Geiger classification, Bragança has a Mediterranean climate with dry summers and mild temperatures (Csb) (Barceló and Nunes, 2009; Bragança, n.d.; Gonçalves *et al.*, 2018).

In the Trás-os-Montes and Alto Douro region and part of the Bragança District (Portugal) (41°29′ 00″ N, 7°11′ 00″ W), the municipality of Mirandela has an area of approximately 674 km² and 23,850 inhabitants (in 2021), with varied relief, including valleys and mountains, and LULC composed mainly of urban fabric, agricultural, and vegetation areas (INE, n.d.; “Mirandela,” 2021). It features a Mediterranean climate type Csa, with hot and dry summers and cool, humid winters (Barceló and Nunes, 2009; “Mirandela,” 2021).

Macedo de Cavaleiros is also part of the Bragança district (41°30′ 00″ N, 6°59′ 00″ W). It has an area of approximately 700 km² and about 16,000 inhabitants (in 2021). It includes industrial, agricultural, forest, natural areas, and urban fabric (INE, n.d.; “Macedo de Cavalheiros,” 2024). Like Bragança, its climate is Csb (Barceló and Nunes, 2009; “Macedo de Cavalheiros,” 2024).

The municipality of Chaves belongs to the Vila Real District and is located in northern Portugal (41°45′ 00″ N, 7°32′ 00″ W). It has an area of approximately 591.32 km² and 41,444 inhabitants (in 2021) (INE, n.d.; “Município Chaves,” n.d.) The LULC comprises urban fabric, industries, commerce, and vegetation areas (Usos *et al.*, 2015). The climate is also classified as Csb (“Climate Data,” n.d.).

Finally, Verín is a municipality in Galicia (Spain) (41°57′ 00″ N, 7°27′ 00″ W). It has 13,817 inhabitants in an area of approximately 94 km² (“Instituto Nacional de Estadística,” n.d.). The climate is also Csb (Barceló and Nunes, 2009; “Clima

Verin," n.d.) and the main LULC occupations are agriculture areas, forested areas, and small-scale urban fabric.

2.2 Data Processing

We processed the satellite images using Google Earth Engine (GEE), a cloud-based platform that speeds up processing time and enhances computational performance. GEE also offers a wide range of satellite products, many of which are pre-processed, including orthorectification and cloud corrections, among other adjustments ("Google Earth Engine," n.d.; Gorelick *et al.*, 2017; Hurni *et al.*, 2017).

2.2.1 MODIS_LST_1km: We used the "MODIS/061/MODIS11A1" collection from the Terra satellite and selected images with daytime overpass times (around 11 am). Although this is not the best time to assess phenomena such as UHI (Anniballe *et al.*, 2014), it coincided with the timing of the other products used from the Sentinel-2 and Landsat-8 satellites. We selected all images from 2018 to 2023 and applied a cloud mask for each to retain only high-quality pixels. We then applied Equation (1) using the LST_Day_1km band to calculate MODIS_LST_1km (Wan, 2013). Finally, we separated the results by season to check the influence of seasonality.

$$\text{MODIS\_LST\_1km} = \text{LST\_Band} \times f_S - K \quad (1)$$

where MODIS_LST_1km = Land Surface Temperature (°C).
LST_Band = LST_Day_1km band.
f_S = scale factor of MODIS (0.02).
K = conversion constant from K to °C (273.15).

2.2.2 NDVI from Sentinel-2 (10m): We selected the "COPERNICUS/S2_SR_HARMONIZED" collection and filtered for the same dates as the selected MODIS products. To ensure we used the highest quality pixels and removed the presence of clouds and their shadows, snow/ice, and water. Additionally, we filtered the LULC band available in this product for classes 4 and 5, representing vegetation and urban/bare areas. We calculated the NDVI using the NIR and RED bands (8 and 4, respectively), applying Equation (2) (Rouse *et al.*, 1973).

$$\text{NDVI} = \frac{(\text{NIR} - \text{RED})}{(\text{NIR} + \text{RED})}, \quad (2)$$

where NDVI = Normalized Difference Vegetation Index.
NIR = reflectance in the near-infrared band.
RED = reflectance in the red band.

2.2.3 Linear Regression: To obtain the appropriate linear regression, it was necessary to resample the NDVI data (Sentinel-2) to a spatial resolution equivalent to MODIS_LST_1km. Initially, to ensure the spatial equivalence of the products, we created a grid based on the pixels of MODIS_LST_1km. We used this grid to identify the spatially coincident pixels in the Sentinel-2 NDVI product and then calculated the average NDVI values within each grid, transforming its scale from 10 m to 1 km.

Next, we calculated the linear regression using MODIS_LST_1km and the NDVI also at 1 km for each analyzed date. Subsequently, we performed the inverse: since we already had the equation for each date, we applied it using the NDVI data at 10 m (in its original size) to obtain the value of MODIS_LST_10m. Additionally, we obtained the Coefficient of Determination (R^2) for each date and evaluated the model's explanatory power. Figure 2 illustrates this process.

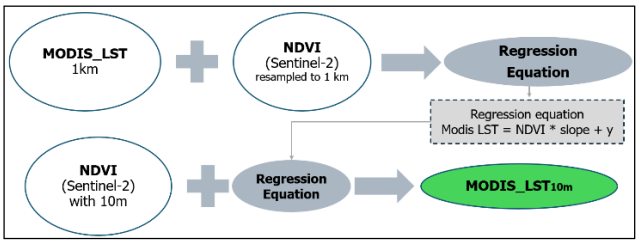

Figure 2. Methodology Applied to Resample Data from the Moderate Resolution Imaging Spectroradiometer (MODIS) from 1 km to 10 m (MODIS_LST_1km and MODIS_LST_10m, respectively).

2.2.4 Validation: We used the product "LANDSAT/LC08/C02/T1_L2" from the Thermal Infrared Sensor (TIRS) of the Landsat-8 satellite. Although the thermal data are obtained at 100 m and resampled to 30 m (US Geological Survey, n.d.), Landsat-8 products offer a considerable availability of free data compared to other satellites with thermal sensors. Its revisit time is 16 days, widely used to generate LST products (Almeida *et al.*, 2021).

Initially, we filtered the products corresponding to the selected MODIS dates and applied a cloud mask to retain only high-quality pixels. To calculate Landsat_LST, we used Band 10, a thermal infrared (TIR) band, applying Equation (3) (US Geological Survey, n.d.).

$$\text{Landsat\_LST} = \text{TIR} \times f_S + O - K \quad (3)$$

where Landsat_LST = Land Surface Temperature (°C).
TIR = reflectance in the thermal infrared band.
f_S = scale factor of Landsat 8 (0.00341802).
O = offset of Landsat 8 (149.0).
K = conversion constant from K to °C (273.15).

To evaluate the correlation between Landsat_LST and MODIS_LST_10m, we ensured that the values corresponded to the same geographic location. To achieve this, we created a grid with 4,981 points based on the centroids of the previously created grid. We included a function in GEE to extract a table containing the values of both parameters at each point for validation. As we applied a series of criteria to select the highest quality pixels, we selected only the dates with at least 50% of the points with available information when extracting data for the point grid.

We applied the Shapiro test in R software and verified that MODIS_LST_10m and Landsat_LST were not normally distributed. Subsequently, we applied Spearman's correlation between the two parameters and evaluated the p-value and the Spearman correlation coefficient (ρ) results.

2.2.5 Analysis of LST and LULC: Using Landsat-8 data on the same validation dates, we calculated the NDVI and EVI. We chose to calculate these vegetation indices from Landsat-8 because they are independent data, meaning they were not used in the construction of the proposed model. For NDVI, we applied Equation (2), using bands 5 (NIR) and 4 (RED), and calculated EVI using Equation (4), including band 2 (BLUE) and the constants defined by the United States Geological Survey (USGS) (Justice *et al.*, 1998; "Landsat Enhanced Vegetation Index," n.d.; Liu and Huete, 1995).

$$\text{EVI} = G \times \frac{(\text{NIR} - \text{RED})}{(\text{NIR} + C1 \times \text{RED} - C2 \times \text{BLUE} + L)}, \quad (4)$$

This contribution has been peer-reviewed. The double-blind peer-review was conducted on the basis of the full paper.
https://doi.org/10.5194/isprs-annals-X-G-2025-729-2025 | © Author(s) 2025. CC BY 4.0 License.

where EVI = Enhanced Vegetation Index.

G = gain factor, which amplifies the difference between the NIR and RED bands, increasing the index's sensitivity in dense vegetation areas. Value used: 2.5.

NIR = reflectance in the near-infrared band.

RED = reflectance in the red band.

C1 e C2 = atmospheric correction coefficients. Values used: 6 and 7.5, respectively.

BLUE = reflectance in the blue band

L = soil adjustment factor, important for areas with low vegetation cover. Value used: 1.

Finally, we used R software to calculate the Spearman correlation (non-parametric data) between MODIS_LST_10m, EVI, and NDVI from Landsat-8 to assess whether higher LST values corresponded to anthropogenic areas and whether areas with vegetation helped regulate temperature.

3. Results

We used 17 images to process the resampling model with linear regression, as they were convergent with the three satellites utilized (MODIS, Sentinel-2, and Landsat-8). The data were separated by season since, for microclimate studies such as UHI, during the spring and summer months, there is a higher solar incidence angle, which can interfere with the results (Santamouris *et al.*, 2015; Wang *et al.*, 2020; Zhou *et al.*, 2010). Of the 17 images, two were from spring, ten from summer, two from autumn, and three from winter. The greater availability of images in summer was associated with a higher presence of clouds in the other seasons. Table 1 presents the days of the images used, the seasons, and the coefficient of determination (R^2) of the proposed resampling model.

The results indicate that the model has greater explainability in summer, considering the R^2 values that ranged between 0.529 and 0.858, with 6 out of the 10 dates showing values above 0.7. This behaviour may be associated with the use of NDVI in model construction, influenced by vegetation density and the higher photosynthetic activity observed during this season, which is driven by increased sunlight incidence and elevated temperatures (Johnson *et al.*, 2018; Pettorelli *et al.*, 2005). Furthermore, the sample size was greater than that of the other seasons, which may be associated with a period when climatic conditions are more stable, characterized by fewer clouds and precipitation, according to the climatic classification of the study area (Barceló and Nunes, 2009).

In autumn, the R^2 was 0.240 and 0.708. The lower value may be associated with a reduction in the photosynthetic activity of vegetation during this season, in addition to changes in color and density due to leaf turnover (Mariën *et al.*, 2019). The values in spring were 0.017 and 0.368, which may be associated with the period when vegetation has not yet fully developed. Additionally, the low amount of data may be explained by the absence of quality pixels on other days during this period (Johnson *et al.*, 2018; Pettorelli *et al.*, 2005). Finally, winter showed the lowest values, possibly associated with climatic conditions such as precipitation, cloud cover, etc. (Hu, 2010; Pinho and Orgaz, 2000). Moreover, it is discussed in the literature that, during this season, to protect themselves from the cold, plants enter a state of dormancy. As a result, using NDVI it is difficult to distinguishing between these vegetations and bare soil, which may have compromised the results (Du *et al.*, 2016; French *et al.*, 2000; French and Inamdar, 2010; Withers and Cooper, 2008). There are also possible associations with the leaf fall of deciduous vegetation, namely during senescencein autumn and winter, which could be linked to this result (Mariën *et al.*, 2019).

Date (MM/DD/YYYY)	Season	Coefficient of Determination (R^2)
05/10/2018	Spring	0.368
07/29/2018	Summer	0.715
09/22/2018	Autumn	0.708
01/05/2019	Winter	0.005
03/26/2019	Spring	0.017
09/02/2019	Summer	0.676
06/23/2020	Summer	0.750
07/18/2020	Summer	0.729
09/11/2020	Summer	0.629
03/15/2021	Winter	0.001
07/28/2021	Summer	0.692
08/22/2021	Summer	0.529
11/10/2021	Autumn	0.240
01/29/2022	Winter	0.003
07/08/2022	Summer	0.773
07/18/2023	Summer	0.858
08/12/2023	Summer	0.785

Table 1. Coefficients of Determination (R^2) obtained in the resampling model of the Moderate Resolution Imaging Spectroradiometer (MODIS) from 1 km to 10 m (MODIS_LST_1km and MODIS_LST_10m, respectively), with date and season.

Considering the model with the highest explanatory power (07/18/2023, in summer), we composed three maps: (a) a cutout of the study area; (b) an LST map using the original spatial resolution of MODIS (MODIS_LST_1km); and (c) a resampled LST map (MODIS_LST_10m) (Figure 3).

In Figure 3 (b), the MODIS_LST_1km product, it is impossible to identify the variations in LULC in the study area in detail. In contrast, the re-sampled model (Figure 3 (c), MODIS_LST_10m product) shows a higher spatial resolution and greater detail of LULC, evidenced by higher LST values in urbanized areas (highlighted in red at the bottom of Figure 3 (c)) and lower values in vegetated areas (in blue, in the central portion of the same map). Analyzing the study area in Figure 3 (a), it is clear that the re-sampled model offers significantly sharper and more precise details than the original resolution in Figure 3 (b).

All analysed dates showed a significant correlation in validating the MODIS_LST_10m model with Landsat_LST data (p-value < 0.05). Although the explainability of the model was not high on all dates, in the validation, the ρ ranged from 0.482 to 0.895, suggesting a moderate to strong correlation between the data. Of the 17 evaluated dates, 14 had ρ values greater than 0.700, indicating the robustness and similarity of the results obtained by the proposed model and the Landsat_LST (Table 2). In the literature, there was also convergence between a downscaling model using Landsat-7 as a validator for MODIS/Sentinel-2 data (Sánchez *et al.*, 2020).

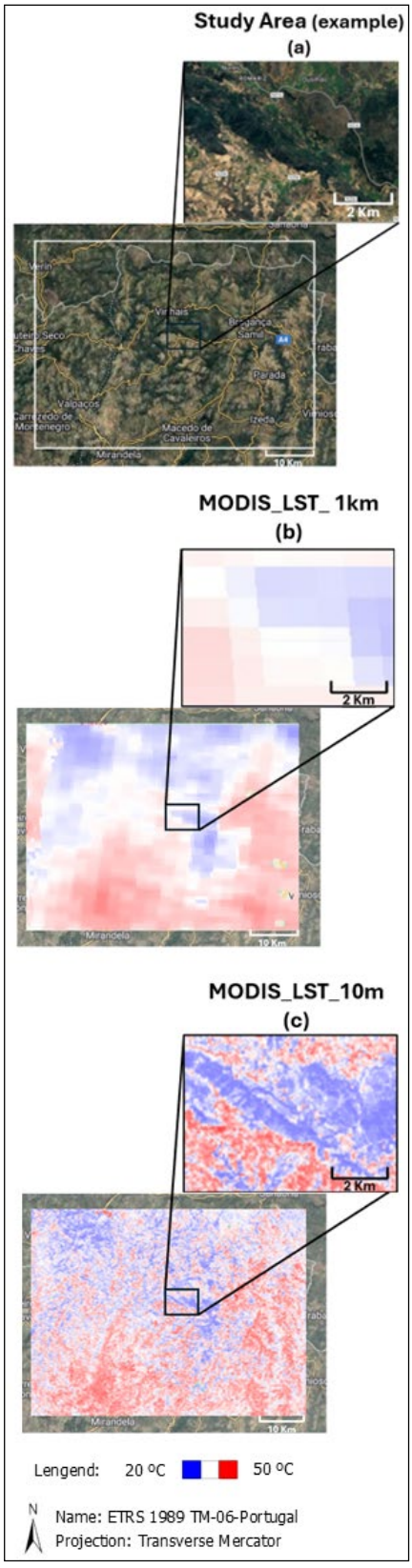

Figure 3. Example of resampling from the Moderate Resolution Imaging Spectroradiometer (MODIS) from 1 km to 10 m, on 07/18/2023 (highest R^2 - summer): (a) study area cutout; (b) Land Surface Temperature (LST) map of MODIS at 1 km (MODIS_LST_1km); and (c) resampled LST map of MODIS at 10 m (MODIS_LST_10m).

Regarding the complementary analyses to understand the correlation between MODIS_LST_10m and EVI and to assess whether vegetation influences surface temperature, all results were significant, except for the date of 05/01/2019 (Table 2). Out of the 16 significant dates, 11 showed ρ values between -0.620 and -0.771, indicating a moderate to strong inverse correlation. Only two dates showed low positive correlations. This result corroborates the literature, which establishes that, in general, LULC areas with vegetation have lower LST values due to their cooling effect (Kramer and Boyer, 1995; Kruger *et al.*, 1983).

Finally, regarding the NDVI data, except 03/15/2021, all other dates were significant (p-value <0.05). The behaviour of the 11 days that showed the highest correlations for the EVI was similar for the NDVI, ranging from -0.649 to -0.811. Even the lowest correlation values were negative, reinforcing the inverse relationship between LST and NDVI, meaning that locations with higher vegetation density exhibit lower surface temperatures and vice versa (Bindajam *et al.*, 2020; Guha *et al.*, 2020) (Table 2).

Date	Season	Spearman Correlation (ρ)		
		Landsat_LST (Validation) (Landsat-8)	Enhanced Vegetation Index (EVI) (Landsat-8)	Normalized Difference Vegetation Index (NDVI) (Landsat-8)
05/10/2018	Spring	0.793	-0.133	-0.462
07/29/2018	Summer	0.807	-0.713	-0.704
09/22/2018	Autumn	0.750	-0.648	-0.705
01/05/2019	Winter	0.823	-0.004	-0.082
03/26/2019	Spring	0.828	0.305	-0.069
09/02/2019	Summer	0.842	-0.655	-0.689
06/23/2020	Summer	0.826	-0.673	-0.722
07/18/2020	Summer	0.788	-0.668	-0.705
09/11/2020	Summer	0.736	-0.636	-0.649
03/15/2021	Winter	0.671	0.426	-0.011
07/28/2021	Summer	0.817	-0.620	-0.687
08/22/2021	Summer	0.827	-0.760	-0.753
11/10/2021	Autumn	0.482	-0.162	-0.373
01/29/2022	Winter	0.676	-0.086	-0.042
07/08/2022	Summer	0.895	-0.743	-0.754
07/18/2023	Summer	0.879	-0.738	-0.811
08/12/2023	Summer	0.842	-0.771	-0.760

Table 2. Spearman Correlation (ρ) results obtained between the resampled model of the Moderate Resolution Imaging Spectroradiometer (MODIS) from 1 km to 10 m (MODIS_LST_1km and MODIS_LST_10m, respectively) and the Landsat_LST (Validation), Enhanced Vegetation Index (EVI), and Normalized Difference Vegetation Index (NDVI) parameters. Results where the correlation was not significant (i.e., p-value > 0.05) are highlighted in red.

In general, these results reaffirm the importance of vegetation in modulating urban temperatures, opening the door for discussions on mitigation and minimization measures for UHI effects through planning strategies (Herrera-Gomez *et al.*, 2017; Zhibin *et al.*, 2015).

4. Conclusions

RS data are crucial for various studies, including monitoring LULC, microclimate, and biomes. One limitation of satellite

data, particularly thermal data, is spatial resolution. The model proposed in this study effectively resampled MODIS data from 1 km to 10 m resolution, particularly during summer when vegetative conditions are more favorable, as reflected in the NDVI from Sentinel-2, which we utilized.

GEE facilitated data acquisition and processing, saving both time and computational resources due to its cloud-based operation.

Our findings revealed a negative correlation between LST data and the VIs in most cases, reinforcing the vegetation's ability to regulate temperature and mitigate UHI effects.

It is important to note that the relationship between LST and VIs depends on local and seasonal climatic conditions. Therefore, conducting detailed analyses in different contexts and considering seasonality is recommended to identify these variations.
However, the reliance on NDVI derived from Sentinel-2 introduced limitations during other seasons, such as winter, when plants enter dormancy, which compromised the accuracy of our estimates.

For future studies, we recommend incorporating indices that rely not solely on vegetation, enhancing effectiveness in seasons with reduced vegetation cover. Additionally, incorporating more specific climatic data, such as soil moisture indices and precipitation, for a more systemic and dynamic analysis between LST and Vis. We suggest complementing this research with data from sources such as Sentinel-3 to refine the methodology and apply it to a broader range of scenarios. Finally, we suggest adding other statistical metrics beyond R^2 to evaluate the robustness of the methodology, such as the mean absolute error (MAE) or the root mean square error (RMSE).

Acknowledgements

This work was supported by national funds through FCT/MCTES (PIDDAC): CIMO, UIDB/00690/2020 (DOI: 10.54499/UIDB/00690/2020) and UIDP/00690/2020 (DOI: 10.54499/UIDP/00690/2020); and SusTEC, LA/P/0007/2020 (DOI: 10.54499/LA/P/0007/2020). The authors are grateful to the Foundation for Science and Technology, I.P., projects UIDB/04683/2020 (https://doi.org/10.54499/UIDB/04683/2020), IDP/04683/2020 (https://doi.org/10.54499/UIDP/04683/2020. Cátia Rodrigues de Almeida was financially supported by Portuguese national funds through FCT (Grant: PRT/BD/153518/2021).

5. References

Agam, N., Kustas, W.P., Anderson, M.C., Li, F., Colaizzi, P.D., 2008. Utility of thermal image sharpening for monitoring field-scale evapotranspiration over rainfed and irrigated agricultural regions. Geophys. Res. Lett. 35, 1–7. https://doi.org/10.1029/2007GL032195

Almeida, C.R. de, Alírio, J., Gonçalves, A., Teodoro, A.C.M., 2023a. Analysis of the urban heat island in Bragança, Portugal, using MODIS data (2003-2022), in: Schulz, K., Nikolakopoulos, K.G., Michel, U. (Eds.), Earth Resources and Environmental Remote Sensing/GIS Applications XIV. SPIE, Amsterdã, p. 15. https://doi.org/10.1117/12.2679713

Almeida, C.R. de, Furst, L., Gonçalves, A., Teodoro, A.C., 2022. Remote Sensing Image-Based Analysis of the Urban Heat Island Effect in Bragança, Portugal. Environ. - MDPI 9. https://doi.org/10.3390/environments9080098

Almeida, C.R. de, Garcia, N., Campos, J.C., Alírio, J., Arenas-Castro, S., Gonçalves, A., Sillero, N., Teodoro, A.C., 2023b. Time-series analyses of land surface temperature changes with Google Earth Engine in a mountainous region. Heliyon 9, e18846. https://doi.org/10.1016/j.heliyon.2023.e18846

Almeida, C.R. de, Teodoro, A.C., Gonçalves, A., 2021. Study of the Urban Heat Island (UHI) Using Remote Sensing Data/Techniques: A Systematic Review. Environments 8, 105. https://doi.org/10.3390/environments8100105

Anniballe, R., Bonafoni, S., Pichierri, M., 2014. Spatial and temporal trends of the surface and air heat island over Milan using MODIS data. Remote Sens. Environ. 150, 163–171. https://doi.org/10.1016/j.rse.2014.05.005

Barceló, A.M., Nunes, L.F., 2009. Iberian Climate Atlas 1971-2000, Atlas Clim{á}tico Ib{é}rico - Iberian Climate Atlas.

Bindajam, A.A., Mallick, J., AlQadhi, S., Singh, C.K., Hang, H.T., 2020. Impacts of Vegetation and Topography on Land Surface Temperature Variability over the Semi-Arid Mountain Cities of Saudi Arabia. Atmosphere (Basel). 11, 762. https://doi.org/10.3390/atmos11070762

Bisquert, M., Sanchez, J.M., Caselles, V., 2016. Evaluation of Disaggregation Methods for Downscaling MODIS Land Surface Temperature to Landsat Spatial Resolution in Barrax Test Site. IEEE J. Sel. Top. Appl. Earth Obs. Remote Sens. 9, 1430–1438. https://doi.org/10.1109/JSTARS.2016.2519099

Bokaie, M., Shamsipour, A., Khatibi, P., Hosseini, A., 2019. Seasonal monitoring of urban heat island using multi-temporal Landsat and MODIS images in Tehran. Int. J. Urban Sci. 23, 269–285. https://doi.org/10.1080/12265934.2018.1548942

Bragança, M. de, n.d. Estratégia Municipal de Adaptação às Alterações Climáticas [WWW Document]. URL https://www.cm-braganca.pt/cmbraganca2020/uploads/writer_file/document/6050/B__8-_Publica__o_do_Plano_Municipal_de_Ambiente.pdf (accessed 10.1.24).

Clima Verin [WWW Document], n.d. URL https://pt.climate-data.org/europa/espanha/galiza/verin-55033/ (accessed 10.6.24).

Climate Data [WWW Document], n.d. URL https://pt.climate-data.org/europa/portugal/chaves/chaves-7128/ (accessed 10.5.24).

Dousset, B., Gourmelon, F., 2003. Satellite multi-sensor data analysis of urban surface temperatures and landcover. ISPRS J. Photogramm. Remote Sens. 58, 43–54. https://doi.org/10.1016/S0924-2716(03)00016-9

Du, H., Song, X., Jiang, H., Kan, Z., Wang, Z., Cai, Y., 2016. Research on the cooling island effects of water body: A case study of Shanghai, China. Ecol. Indic. 67, 31–38. https://doi.org/10.1016/j.ecolind.2016.02.040

EPA - United States Environmental Protection Agency, n.d. Ilhas de calor [WWW Document]. URL http://www.epa.gov/heat-islands (accessed 10.13.24).

French, A.., Schmugge, T.., Kustas, W.., 2000. Discrimination of Senescent Vegetation Using Thermal Emissivity Contrast. Remote Sens. Environ. 74, 249–254. https://doi.org/10.1016/S0034-4257(00)00115-2

French, A.N., Inamdar, A., 2010. Land cover characterization for hydrological modelling using thermal infrared emissivities. Int. J. Remote Sens. 31, 3867–3883. https://doi.org/10.1080/01431161.2010.483491

Gaitán, J.J., Bran, D., Oliva, G., Ciari, G., Nakamatsu, V., Salomone, J., Ferrante, D., Buono, G., Massara, V.,

Humano, G., Celdrán, D., Opazo, W., Maestre, F.T., 2013. Evaluating the performance of multiple remote sensing indices to predict the spatial variability of ecosystem structure and functioning in Patagonian steppes. Ecol. Indic. 34, 181–191. https://doi.org/10.1016/j.ecolind.2013.05.007

Gonçalves, A., Ornellas, G., Ribeiro, A.C., Maia, F., Rocha, A., Feliciano, M., 2018. Urban cold and Heat Island in the City of Bragança (Portugal). Climate 6, 1–14. https://doi.org/10.3390/cli6030070

Google Earth Engine [WWW Document], n.d. URL https://earthengine.google.com (accessed 10.1.24).

Gorelick, N., Hancher, M., Dixon, M., Ilyushchenko, S., Thau, D., Moore, R., 2017. Google Earth Engine: Planetary-scale geospatial analysis for everyone. Remote Sens. Environ. 202, 18–27. https://doi.org/10.1016/j.rse.2017.06.031

Grover, A., Singh, R.B., 2016. Monitoring Spatial patterns of land surface temperature and urban heat island for sustainable megacity: A case study of Mumbai, India, using landsat TM data. Environ. Urban. ASIA 7, 38–54. https://doi.org/10.1177/0975425315619722

Guha, S., Govil, H., Diwan, P., 2020. Monitoring LST-NDVI Relationship Using Premonsoon Landsat Datasets. Adv. Meteorol. 2020. https://doi.org/10.1155/2020/4539684

Guillevic, P., Göttsche, F., Nickeson, J., Hulley, G., Ghent, D., Yu, Y., Trigo, I., Hook, S., Sobrino, J.A., Remedios, J., Román, M., Camacho, F., 2018. Land surface temperature product validation best practice protocol version 1.1. Best Pract. Satell. L. Prod. Valid. (p. 60) L. Prod. Valid. Subgr. doi, 58. https://doi.org/10.5067/doc/ceoswgcv/lpv/lst.001

Hall, D.K., Comiso, J.C., Digirolamo, N.E., Shuman, C.A., Key, J.R., Koenig, L.S., 2012. A satellite-derived climate-quality data record of the clear-sky surface temperature of the greenland ice sheet. J. Clim. 25, 4785–4798. https://doi.org/10.1175/JCLI-D-11-00365.1

Herrera-Gomez, S.S., Quevedo-Nolasco, A., Pérez-Urrestarazu, L., 2017. The role of green roofs in climate change mitigation. A case study in Seville (Spain). Build. Environ. 123, 575–584. https://doi.org/10.1016/j.buildenv.2017.07.036

Hu, D., 2010. Analysis of surface radiation budget during the summer and winter in the metropolitan area of Beijing, China. J. Appl. Remote Sens. 4, 043513. https://doi.org/10.1117/1.3374329

Hulley, G.C., Ghent, D., Göttsche, F.M., Guillevic, P.C., Mildrexler, D.J., Coll, C., 2019. Land Surface Temperature, Taking the Temperature of the Earth. https://doi.org/10.1016/b978-0-12-814458-9.00003-4

Hurni, K., Heinimann, A., Würsch, L., 2017. Google Earth Engine Image Pre-processing Tool : Background and Methods 12.

Imhoff, M.L., Zhang, P., Wolfe, R.E., Bounoua, L., 2010. Remote sensing of the urban heat island effect across biomes in the continental USA. Remote Sens. Environ. 114, 504–513. https://doi.org/10.1016/j.rse.2009.10.008

INE, I.N. de E., n.d. Censos 2021 [WWW Document]. URL https://censos.ine.pt/xportal/xmain?xpgid=censos21_main&xpid=CENSOS21&xlang=pt (accessed 9.10.24).

Instituto Nacional de Estadística [WWW Document], n.d. URL https://www.ine.es/dyngs/AYU/en/index.htm?cid=118 (accessed 10.6.24).

Johnson, H.E., Gustine, D.D., Golden, T.S., Adams, L.G., Parrett, L.S., Lenart, E.A., Barboza, P.S., 2018. NDVI exhibits mixed success in predicting spatiotemporal variation in caribou summer forage quality and quantity. Ecosphere 9. https://doi.org/10.1002/ecs2.2461

Justice, C.O., Vermote, E., Townshend, J.R.G., Defries, R., Roy, D.P., Hall, D.K., Salomonson, V.V., Privette, J.L., Riggs, G., Strahler, A., Lucht, W., Myneni, R.B., Knyazikhin, Y., Running, S.W., Nemani, R.R., Zhengming Wan, Huete, A.R., van Leeuwen, W., Wolfe, R.E., Giglio, L., Muller, J., Lewis, P., Barnsley, M.J., 1998. The Moderate Resolution Imaging Spectroradiometer (MODIS): land remote sensing for global change research. IEEE Trans. Geosci. Remote Sens. 36, 1228–1249. https://doi.org/10.1109/36.701075

Kramer, P., Boyer, J., 1995. Water Relations of Plants and Soils, 1st Editio. ed.

Kruger, F.J., Mitchell, D.T., Jarvis, J.U.M., 1983. Mediterranean-Type Ecosystems, Ecological Studies. Springer Berlin Heidelberg, Berlin, Heidelberg. https://doi.org/10.1007/978-3-642-68935-2

Landsat Enhanced Vegetation Index [WWW Document], n.d. URL https://www.usgs.gov/landsat-missions/landsat-enhanced-vegetation-index (accessed 10.11.24).

Lillesand, T., Kiefer, R.W., Chipman, J., 2015. Remote Sensing and Image Interpretation, 7th ed. Wiley.

Liu, H.Q., Huete, A., 1995. A feedback based modification of the NDVI to minimize canopy background and atmospheric noise. IEEE Trans. Geosci. Remote Sens. 33, 457–465. https://doi.org/10.1109/TGRS.1995.8746027

Luvall, J.C., Quattrochi, D.A., Rickman, D.L., Estes, M.G., 2015. Boundary Layer (Atmospheric) and Air Pollution: Urban Heat Islands, Second Edi. ed, Encyclopedia of Atmospheric Sciences: Second Edition. Elsevier. https://doi.org/10.1016/B978-0-12-382225-3.00442-4

Macedo de Cavalheiros [WWW Document], 2024. URL https://www.cm-macedodecavaleiros.pt/pages/657 (accessed 10.5.24).

Mariën, B., Balzarolo, M., Dox, I., Leys, S., Lorène, M.J., Geron, C., Portillo-Estrada, M., AbdElgawad, H., Asard, H., Campioli, M., 2019. Detecting the onset of autumn leaf senescence in deciduous forest trees of the temperate zone. New Phytol. 224, 166–176. https://doi.org/10.1111/nph.15991

Mirandela [WWW Document], 2021. URL https://www.cm-mirandela.pt/pages/300 (accessed 10.5.24).

Mirzaei, M., Verrelst, J., Arbabi, M., Shaklabadi, Z., Lotfizadeh, M., 2020. Urban heat island monitoring and impacts on citizen’s general health status in Isfahan metropolis: A remote sensing and field survey approach. Remote Sens. 12, 1–17. https://doi.org/10.3390/RS12081350

Miura, T., Huete, A.R., Yoshioka, H., Holben, B.N., 2001. An error and sensitivity analysis of atmospheric resistant vegetation indices derived from dark target-based atmospheric correction. Remote Sens. Environ. 78, 284–298. https://doi.org/10.1016/S0034-4257(01)00223-1

Município Chaves [WWW Document], n.d. URL https://www.chaves.pt/pages/142 (accessed 10.5.24).

NASA, n.d. Terra & Aqua Moderate Resolution Imaging Spectroradiometer (MODIS) [WWW Document]. URL https://ladsweb.modaps.eosdis.nasa.gov/missions-and-measurements/modis/ (accessed 10.14.24).

Oke, T.R., 1982. The energetic basis of the urban heat island. Q. J. R. Meteorol. Soc. 108, 1–24. https://doi.org/10.1002/qj.49710845502

Pettorelli, N., Vik, J.O., Mysterud, A., Gaillard, J.-M., Tucker, C.J., Stenseth, N.C., 2005. Using the satellite-derived NDVI to assess ecological responses to environmental change. Trends Ecol. Evol. 20, 503–510. https://doi.org/10.1016/j.tree.2005.05.011

Pinho, O.S., Orgaz, M.D.M., 2000. The urban heat island in a small city in coastal Portugal. Int. J. Biometeorol. 44, 198–

203. https://doi.org/10.1007/s004840000063
Rouse, J.W., Haas, R.H., Schell, J.A., Deering, D.W., 1973. Monitoring vegetation systems in the great plains with ERTS. 3rd ERTS Symp. 309–317.
Sánchez, J.M., Galve, J.M., González-Piqueras, J., López-Urrea, R., Niclòs, R., Calera, A., 2020. Monitoring 10-m LST from the Combination MODIS/Sentinel-2, Validation in a High Contrast Semi-Arid Agroecosystem. Remote Sens. 12, 1453. https://doi.org/10.3390/rs12091453
Santamouris, M., Cartalis, C., Synnefa, A., 2015. Local urban warming, possible impacts and a resilience plan to climate change for the historical center of Athens, Greece. Sustain. Cities Soc. 19, 281–291. https://doi.org/10.1016/j.scs.2015.02.001
Tomlinson, C.J., Chapman, L., Thornes, J.E., Baker, C., 2011. Remote sensing land surface temperature for meteorology and climatology: a review. Meteorol. Appl. 18, 296–306. https://doi.org/10.1002/met.287
US Geological Survey, n.d. Landsat Missions [WWW Document]. URL https://www.usgs.gov/core-science-systems/nli/landsat/landsat-8?qt-science_support_page_related_con=0#qt-science_support_page_related_con (accessed 9.12.24).
Usos, G., Ocupa, C.D.E., Em, D.O.S., Em, D.O.S., Em, D.O.S., De, D.O.S., 2015. Revisão do Plano Diretor Municipal de Chaves.
Voogt, J.., Oke, T.., 2003. Thermal remote sensing of urban climates. Remote Sens. Environ. 86, 370–384. https://doi.org/10.1016/S0034-4257(03)00079-8
Wan, Z., 2013. MODIS Collection 6.1 (C61) Product User Guide. Qual. Assur. 1. https://doi.org/https://doi.org/10.5067/MODIS/MOD11A1.061
Wang, M., Zhang, Zhengjia, Hu, T., Wang, G., He, G., Zhang, Zhaoming, Li, H., Wu, Z., Liu, X., 2020. An Efficient Framework for Producing Landsat-Based Land Surface Temperature Data Using Google Earth Engine. IEEE J. Sel. Top. Appl. Earth Obs. Remote Sens. 13, 4689–4701. https://doi.org/10.1109/JSTARS.2020.3014586
Weng, Q., Fu, P., 2014. Modeling diurnal land temperature cycles over Los Angeles using downscaled GOES imagery. ISPRS J. Photogramm. Remote Sens. 97, 78–88. https://doi.org/10.1016/j.isprsjprs.2014.08.009
Weng, Q., Lu, D., Schubring, J., 2004. Estimation of land surface temperature-vegetation abundance relationship for urban heat island studies. Remote Sens. Environ. 89, 467–483. https://doi.org/10.1016/j.rse.2003.11.005
Withers, P.C., Cooper, C.E., 2008. Dormancy, in: Encyclopedia of Ecology. Elsevier, pp. 952–957. https://doi.org/10.1016/B978-008045405-4.00503-6
Zhibin, R., Haifeng, Z., Xingyuan, H., Dan, Z., Xingyang, Y., 2015. Estimation of the Relationship Between Urban Vegetation Configuration and Land Surface Temperature with Remote Sensing. J. Indian Soc. Remote Sens. 43, 89–100. https://doi.org/10.1007/s12524-014-0373-9
Zhou, D., Xiao, J., Bonafoni, S., Berger, C., Deilami, K., Zhou, Y., Frolking, S., Yao, R., Qiao, Z., Sobrino, J.A., 2019. Satellite remote sensing of surface urban heat islands: Progress, challenges, and perspectives. Remote Sens. 11, 1–36. https://doi.org/10.3390/rs11010048
Zhou, J., Hu, D., Weng, Q., 2010. Analysis of surface radiation budget during the summer and winter in the metropolitan area of Beijing, China. J. Appl. Remote Sens. 4, 043513. https://doi.org/10.1117/1.3374329